Supplementary material for: "Optimizing Brownian escape rates by potential shaping"

Marie Chupeau,[1] Jannes Gladrow,[2] Alexei Chepelianskii,[3] Ulrich F. Keyser,[2] and Emmanuel Trizac[1]

[1] *LPTMS, CNRS, Univ. Paris-Sud, Université Paris-Saclay, 91405 Orsay, France*
[2] *Cavendish Laboratory, University of Cambridge, Cambridge CB3 0HE, United Kingdom*
[3] *Laboratoire de Physique des Solides, CNRS, Univ. Paris-Sud, Université Paris-Saclay, 91405 Orsay, France*

Starting with setting the framework in section I and being interested in mean-first passage times, we bring to the fore the key feature of potential antisymmetry. We then present in Section II the experimental setup and techniques. We show in section III that for overdamped dynamics, the optimal potential is necessarily antisymmetric, as soon as the constraint on the potential is compatible with such a property. Second, we optimize in section IV the potential within constraint A (bounded potential). We then show in section V that the escape time boost is not specific to the one dimensional setting on which our attention is mainly focussed, but also holds in higher dimensions. We finally present the general underdamped framework, with analytical asymptotic results (section VI) and the Finite Element Method technique used for numerical resolution (section VII).

I. THE GENERAL FRAMEWORK AND A KEY PROPERTY OF THE MEAN FIRST PASSAGE TIME

The whole analysis is performed at the level of the Langevin equation [1, 2] for the motion of a Brownian object in the force field stemming from an external static potential $U(x)$. We mostly focus on the one dimensional formulation (see Section V otherwise), for which the position x of a 'particle' with mass m obeys

$$m\ddot{x} \,=\, -\gamma m\dot{x} \,-\, U'(x) \,+\, m\gamma\,\sqrt{D}\,\eta(t) \tag{S1}$$

where γ denotes the friction coefficient, $U(x)$ the potential in which the particle evolves, $D = k_BT/(m\gamma)$ the diffusion coefficient, and k_BT is thermal energy. The random term $\eta(t)$ is a standard delta-correlated noise: $\langle\eta(t)\eta(t')\rangle = 2\delta(t-t')$. Time and space derivatives are denoted by a point and a dash respectively. In the overdamped limit, met with large friction coefficients, the inertial term becomes negligible, and the equation of motion simplifies into:

$$\dot{x} = -\frac{1}{m\gamma}U'(x) + \sqrt{D}\,\eta(t), \tag{S2}$$

where $1/(m\gamma)$ is the mobility. Statistical properties of the x-evolution are enclosed in the probability density function (pdf) $P(x,t)$ to find the particle at the point x at time t, starting from a given initial state. The pdf obeys the Smoluchowski equation

$$\partial_t P = \frac{1}{m\gamma}\partial_x(PU') + D\,\partial_x^2 P. \tag{S3}$$

In the more general underdamped framework associated to Eq. (S1), the pdf $K(x,v,t)$ (such that $P = \int K dv$) obeys the so-called Kramers equation [2], given in Eq. (S35) below.

For a given static external potential $U(x)$, a classic argument [2, 3] yields the mean first-passage time $\tau[U(x)]$ provided by Eq. (1) in the main text. Before embarking in the analysis, it is worth discussing the ensuing interesting antisymmetry property of the mean first passage time, that plays a fundamental role in our treatment [4]:

$$\tau[U(x)] \,=\, \tau[-U(1-x)]. \tag{S4}$$

This is a mere consequence of Eq. (1); it implies that the two profiles shown in Fig. S1 lead to the same mean first passage time at $x = 1$. While this may be surprising at first, it appears that it is completely equivalent to first get out of the well and then slide to the exit (Fig. S1(a)) or first slide down and then climb a steep slope (Fig. S1(b)). Indeed, if the slide part is identical between (a) and (b), the well part is different. In (a), the particle is blocked leftwards by a reflecting wall, acting like an infinitely high potential, whereas in (b), the well is less confining, because of its left part, which is the slide. Following Kramers-like phenomenology subsumed in Fig. 1 in the main text, the particle should (and does) escape quicker from the most confining well of (a). However, once escaped from the well, the particle can fall back down into it in (a) (recrossings) whereas it cannot in (b) as the top of the well is absorbing. It turns out that the two effects (well escape and recrossing) exactly compensate and lead to the identity (S4).

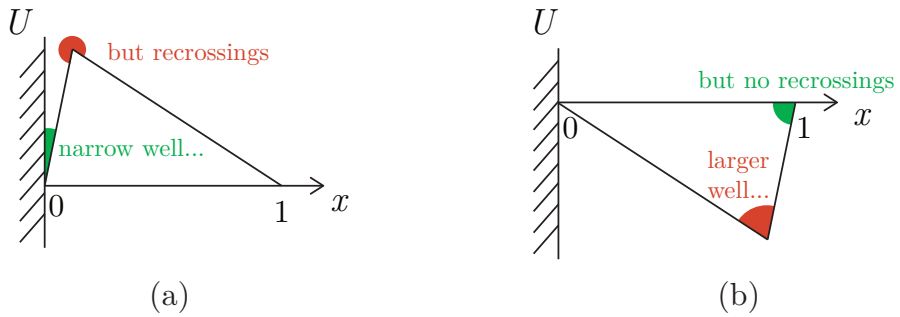

FIG. S1: Illustration of the generic identity (S4). These two potentials yield the same mean exit time, stemming from a remarkable compensation between the difference of escape time from the two wells and the recrossing occurrence. The particle starts from $x = 0$ at the reflecting wall and is absorbed at $x = 1$.

II. EXPERIMENTS

We used an Ytterbium fiber laser (YLM-5-1064-LP, IPG Photonics) at 2.5 W power with a wavelength of 1064 nm. To shape the beam, we used a liquid crystal SLM (LCOS X10468, Hamamatsu) with a refresh rate of 60 Hz. Further details about the setup can be found in previous publications [5]. The colloidal particles had a nominal diameter of 350 nm, consisted of polystyrene and are commercially available from Polysciences Inc. The colloids were dispersed in a measurement buffer (3 mM KCl, 0.5xTris at pH 8) and sonicated prior to the experiment. The microfluidic mask was cast in Polydimethylsiloxane (PDMS) and featured channels with dimensions of $25 \times 1 \times 1\,\mu$m. Both ends of the channel are connected by macroscopic channels to swiftly equilibrate pressure differences.

As stated in the main text, the experimental N-shaped potential represented on Fig. 3(d), corresponding to the rightmost star of Fig. 2(d), was created by a combination of a single point trap providing the initial potential well and three line traps with phase-gradients and lengths given by the following table.

Type	I	x_c	L	p
Line	0.2	$-0.91\,\mu$m	$2\,\mu$m	1
Point	0.09	$0\,\mu$m	N.A.	N.A.
Line	1.1	$8.05\,\mu$m	$16\,\mu$m	0.1
Line	0.6	$17.45\,\mu$m	$3\,\mu$m	-1

FIG. S2: Parameters of the *Red tweezers program* [6] used to create the N-shaped barrier

I denotes the relative intensities, x_c represents the centre of the respective trap, L stands for the length of the line trap, while $p \in [-1, 1]$ is a relative measure for the phase-gradient of a line trap.

This combination of parameters is the one with which we obtained the lowest experimental rescaled mean exit time. We also report another experimental potential that yields a slightly higher mean exit time, but presents a better efficiency (that is to say a better balance acceleration - potential amplitude). This second potential profile, represented in Fig. S3, corresponds to the leftmost star on Fig. 2(d) in the main text. It is less N-shaped than the experimental profile of Fig. 2(d), but displays less interference oscillations, preventing the colloid to lose time in intermediary potential wells before exiting.

III. ANTISYMMETRY OF THE OPTIMAL POTENTIAL

In the overdamped regime, the mean exit time is given by Eq. (1) in the main text and is the same for a general potential $U(x)$ and for $-U(1-x)$, see section I. Using this property, we can write

$$\tau^2[U(x)] = \tau[U(x)]\,\tau[-U(1-x)] = \int_0^1 dx\, e^{-U(x)} \int_x^1 dy\, e^{U(y)} \times \int_0^1 dx'\, e^{U(1-x')} \int_{x'}^1 dy'\, e^{-U(1-y')}. \tag{S5}$$

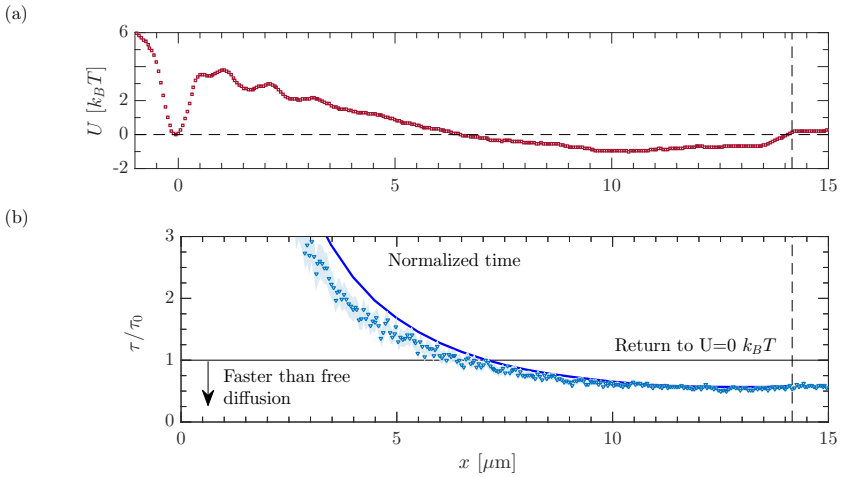

FIG. S3: (a) Experimental potential profile corresponding to the leftmost star on Fig. 2(d) of the main text. The interval of interest is between $x = 0$ and the vertical dashed line. (b) Measured first-passage times for the potential profile (a) normalized by the zero-potential fit $\langle\tau_0\rangle$. The continuous curve is the theoretical calculation of $\tau[U]$ following from Eq. (1) in the main text, where U is the measured potential shown in panel a). Both (a) and (b) share their x axis.

We use the Cauchy-Schwarz inequality for the following scalar product

$$\langle f|g\rangle = \int_0^1 f(x)g(x)\,dx \tag{S6}$$

and the associated norm $||f|| = \sqrt{\langle f|f\rangle}$. This yields

$$\tau^2[U(x)] \geqslant \left(\int_0^1 dx\, e^{-\frac{U(x)-U(1-x)}{2}} \sqrt{\int_x^1 dy e^{U(y)} \int_x^1 dy' e^{-U(1-y')}}\right)^2. \tag{S7}$$

We invoke again the Cauchy-Schwarz inequality for the integral scalar product on $[x, 1]$ to obtain

$$\tau^2[U(x)] \geqslant \left(\int_0^1 dx\, e^{-\frac{U(x)-U(1-x)}{2}} \int_x^1 dy\, e^{\frac{U(y)-U(1-y)}{2}}\right)^2 = \tau^2\left[\frac{U(x)-U(1-x)}{2}\right]. \tag{S8}$$

This function $[U(x) - U(1 - x)]/2 = U_a(x)$ is the original potential $U(x)$, anti-symmetrized with respect to $x = 1/2$. It means that

$$\tau^2[U(x)] \geqslant \tau^2[U_a(x)], \tag{S9}$$

namely that the mean exit time associated with a potential U is always larger than the mean exit time associated with its anti-symmetrized version U_a. So, provided that the ensemble of potentials allowed by the regularization constraint is stable under this antisymmetry operation (*i.e.* if U is in this ensemble, so is U_a), the optimal potential is necessarily antisymmetric itself.

IV. OPTIMIZATION WITHIN CONSTRAINT A

With constraint A, the potential is such that for all $x \in [0, 1]$, $U_{\min} \leqslant U(x) \leqslant U_{\max}$. The optimal profile A that we are looking for can be split into three regions (see Fig. S4): region ① where it is equal to the upper bound $U_{\max}$, region ② where it is equal to the lower bound $U_{\min}$ and region ③ where it is not constrained ($U_{\min} < U(y) < U_{\max}$). A priori, these three regions can be non-connected. In order to determine the optimal profile A, we use variational calculus, and compute

$$\delta\tau = \int_0^1 dx \int_0^1 dy\, \Theta(y - x)e^{U(y)-U(x)}(\delta U(y) - \delta U(x)) \tag{S10}$$

where Θ is the Heaviside step function. Outside of the constrained regions ① and ②, this variation $\delta\tau$ is zero at the optimum, yielding

$$e^{U(y)} \int_0^y dx\, e^{-U(x)} = e^{-U(y)} \int_y^1 dx\, e^{U(x)}. \tag{S11}$$

We differentiate once this equation with respect to y to get

$$\int_0^y dx\, e^{-U(x)} = -\frac{e^{-U(y)}}{U'(y)} \tag{S12}$$

and once more

$$\frac{d}{dy}\left(\frac{1}{U'(y)}\right) = 0. \tag{S13}$$

Equation (S13) indicates that the optimal potential A is linear in region ③, with a negative slope as follows from Eq. (S12). It can be shown that optimal potential A displays the sequence region ①, region ③ and region ②. Regions ①, ② and ③ are therefore connected and the optimal potential has the generic shape represented in Fig. S4. As for the abscissas x^* and y^* of the intersection between these three regions, they can be extracted straightforwardly from Eq. (S11) and (S12).

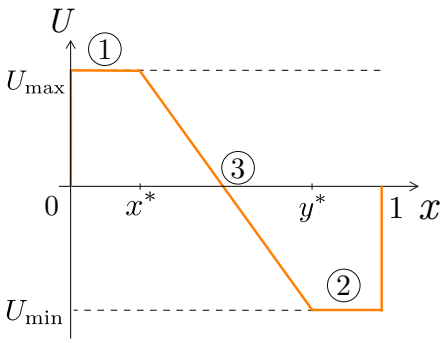

FIG. S4: Sketch of optimal potential A, with illustration of regions ①, ② and ③.

V. BEYOND ONE SPATIAL DIMENSION

Our problem is readily generalized to an arbitrary space dimension d. We focus on the mean time that an overdamped walker needs to escape from a (hyper)sphere, starting from its center. We consider a potential with rotational symmetry $U(r)$, and $P(r,t)$ the associated probability density function of the particle. The latter obeys a Fokker-Planck equation

$$\partial_t P = \frac{1}{\gamma\, r^{d-1}} \partial_r \left(r^{d-1} P \partial_r U\right) + \frac{D}{r^{d-1}} \partial_r \left(r^{d-1} \partial_r P\right). \tag{S14}$$

A derivation using standard techniques leads to the general expression in dimension d

$$\tau = \int_0^1 dr\, r^{d-1} e^{-U(r)} \int_r^1 \frac{dr'}{r'^{d-1}}\, e^{U(r')} \tag{S15}$$

where the mean exit time is rescaled by R^2/D with R the radius of the sphere. This expression can be recast into a one-dimensional-like expression

$$\tau = \int_0^1 dr\, e^{-V(r)} \int_r^1 dr' e^{V(r')} \tag{S16}$$

with the effective potential $V(r)$ defined as

$$V(r) = U(r) - (d-1)\ln r. \tag{S17}$$

The logarithmic contribution above invalidates the antisymmetry property discussed in section I for one-dimensional potentials. Here, the mean exit time associated with the potential $-U(1-r)$ is not the same as its counterpart for $U(r)$.

Minimizing τ in (S16) we obtain the following equation

$$e^{U(r)} \int_0^r dr' \left(\frac{r'}{r}\right)^{d-1} e^{-U(r')} = e^{-U(r)} \int_r^1 dr' \left(\frac{r}{r'}\right)^{d-1} e^{U(r')} \tag{S18}$$

and its derivative with respect to r

$$\int_0^r dr' r'^{d-1} e^{-U(r')} = \frac{r^{d-1} e^{-U(r)}}{\frac{d-1}{r} - U'(r)}. \tag{S19}$$

As previously, taking the derivative with respect to r of equation (S19) leads to the following form for the unconstrained part of the optimal potential

$$U(r) = (d-1)\ln r - Ar + B, \tag{S20}$$

with $A > 0$. The logarithmic component can be viewed as an entropic force that tends to bias the displacement towards the regions of higher accessible configuration space, namely the regions of large radii.

We can investigate more thoroughly the shape of the optimal potential in the particular case of dimension 2. The following analysis could be easily transposed to dimensions 3 and higher. The constants A and B can be determined by continuity of the optimal potential at the transition point between the upper bound and the intermediary portion (in x^*) on the one hand, and the intermediary portion and the lower bound (in y^*) on the other hand. The generic profile is

$$U(r) = \begin{cases} U_{\max} & \text{if } r \in [0, x^*] \\ U_{\max} + \ln r - \ln x^* - \dfrac{U_{\max} - \ln x^* - U_{\min} + \ln y^*}{y^* - x^*}(r - x^*) & \text{if } r \in]x^*, y^*[\\ U_{\min} & \text{if } r \in [y^*, 1]. \end{cases} \tag{S21}$$

Following the same lines as for the one-dimensional case, i.e. injecting this potential profile into equations (S18) and (S19), we obtain

$$x^* = -2y^* \ln y^* \tag{S22}$$

$$\frac{x^*}{2} = \frac{y^* - x^*}{U_{\max} - \ln x^* - U_{\min} + \ln y^*}. \tag{S23}$$

Combining these two equations and setting again $\Delta U = U_{\max} - U_{\min}$, we get

$$2 + \Delta U + \ln\left(\frac{1}{2\ln\left(\frac{1}{y^*}\right)}\right) = \frac{1}{\ln\left(\frac{1}{y^*}\right)}. \tag{S24}$$

If we define

$$Y^* = \frac{1}{\ln\left(\frac{1}{y^*}\right)}, \tag{S25}$$

we get the simple yet implicit relation

$$2 + \Delta U - \ln 2 + \ln Y^* = Y^*. \tag{S26}$$

This equation has two solutions, one for $Y^* < 1$ and one for $Y^* > 1$, corresponding respectively to $y^* < e^{-1}$ and $y^* > e^{-1}$. Moreover, by definition, $x^* < y^*$, which implies $y^* > e^{-0.5}$ because of equation (S22). The only relevant solution is then $Y^* > 1$.

In order to solve the implicit equation (S26), we study its asymptotics when $\Delta \gg 1$. In this case, Y^* is also large compared to 1 and then $\ln Y^* \ll Y^*$. We deduce from equation (S26) the leading term of Y^* and the first corrections

$$Y^* = \Delta U + \ln \Delta U + 2 - \ln 2 + o(1), \tag{S27}$$

therefore

$$y^* = e^{-\frac{1}{Y^*}} \simeq e^{-\frac{1}{\Delta U + \ln \Delta U + 2 - \ln 2}} \tag{S28}$$

$$x^* = \frac{2e^{-\frac{1}{\Delta U + \ln \Delta U + 2 - \ln 2}}}{\Delta U + \ln \Delta U + 2 - \ln 2}. \tag{S29}$$

At large ΔU, this reduces to

$$y^* = 1 - \frac{1}{\Delta U + \ln \Delta U + 2 - \ln 2} \tag{S30}$$

$$x^* = \frac{2}{\Delta U + \ln \Delta U + 2 - \ln 2}. \tag{S31}$$

Note that the relation $y^* = 1 - x^*$ that was verified in one dimension does not hold in two dimensions, even asymptotically. The accuracy of the developments (S28) and (S30) is tested on figure S5(a) as a function of ΔU. The shape of the optimal potential in two dimensions is represented on figure S5(b). The asymmetry introduced by the entropic force, that pushes the particle away from the center, has two manifestations: the non-linearity of the intermediary portion and the size of the plateau on $U_{\min}$ that is shorter than the size of the plateau on $U_{\max}$, see Fig. S5.

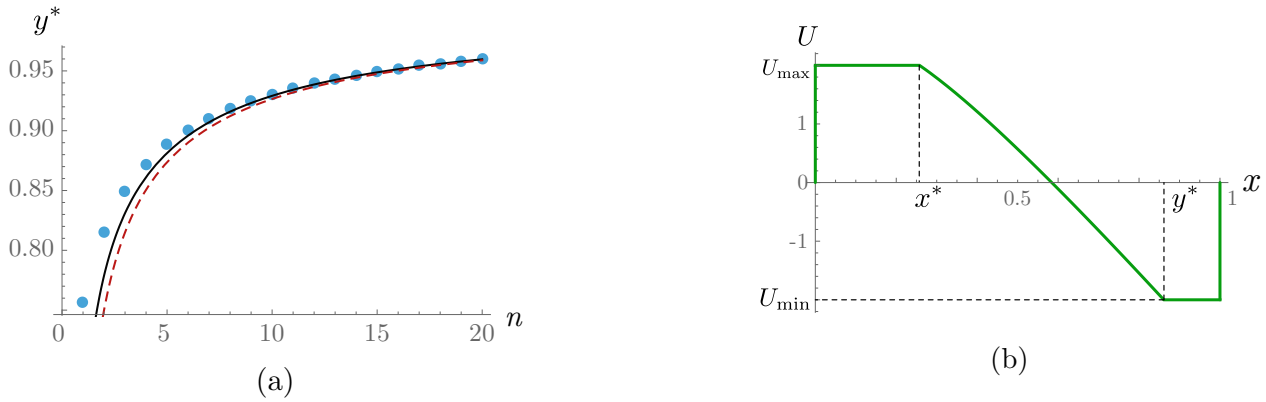

FIG. S5: (a) Comparison between the exact value of y^*, obtained by solving numerically Eq. (S26) (blue circles), and the approached expressions (S28) (black line) and (S30) (red dashed line). (b) Example of optimal potential profile in two dimensions, with the bounds $U_{\max} = -U_{\min} = 2$.

The mean exit time corresponding to this optimal potential can be expressed using the generic shape given in Eq. (S21) as well as Eqs. (S22) and (S23)

$$\tau = \frac{x^* y^*}{4} + \frac{1 - y^{*2}}{4}. \tag{S32}$$

The asymptotics of this expression for potential difference $\Delta U \gg 1$ can be extracted using Eqs. (S30) and (S31)

$$\tau = \frac{1}{\Delta U} + o\left(\frac{1}{\Delta U}\right), \tag{S33}$$

which means that the Heisenberg-like relation $\tau \Delta U \sim 1$ still holds at large ΔU in dimensions larger than 1.

VI. UNDERDAMPED TREATMENT: ANALYTICS

Within the underdamped treatment (Eq. (S1)), a natural rescaling for the velocity is $\widetilde{v} = v\sqrt{m/(kT)}$. Whereas there was only one timescale in the overdamped problem (the diffusion time $t_d = L^2/D$), there is now a second

(ballistic) one $t_b = L\sqrt{m/(kT)}$, related to the velocity scale. We accordingly define two dimensionless times,

$$\widetilde{t} = \frac{t}{t_d}, \qquad \widetilde{\widetilde{t}} = \frac{t}{t_b} = \widetilde{\gamma}\widetilde{t}. \tag{S34}$$

Rescaling with t_b is natural for calculations, as it is consistent with the rescalings of space and velocity already chosen. We use the resulting $\widetilde{\widetilde{t}}$ in the following calculations. However, rescaling with t_d is adapted for comparison with the overdamped case. In particular, within this second rescaling, the limit of the mean exit time at large γ is a constant ($\widetilde{\tau} \to 1/2$), making the large damping asymptotics easier to visualize. We adopted this second rescaling in the main text. As previously, we only work with rescaled variables and then drop tildes, except for the time, where we keep the tilde (or double tilde) to avoid confusion.

The underdamped probability density function $K\left(x, v, \widetilde{\widetilde{t}}\right)$, obeys the Kramers equation

$$\partial_{\widetilde{\widetilde{t}}} K + v\partial_x K - \partial_x U \partial_v K = \gamma \partial_v \left(vK + \partial_v K\right). \tag{S35}$$

The starting point $x = 0$ and the initial velocity v, distributed as the equilibrium Gaussian $\mathcal{N}(v)$

$$\mathcal{N}(v) = \frac{1}{\sqrt{2\pi}} e^{-\frac{v^2}{2}}, \tag{S36}$$

are implicit in the following. Solving this equation for the mean exit time is much more complicated in the underdamped regime and no analytical general result is known. However, the mean exit time can be related to the particle density function. In order to show that, we first introduce the Green function

$$G(x, v) = \int_0^{+\infty} d\widetilde{\widetilde{t}}\, K\left(x, v, \widetilde{\widetilde{t}}\right). \tag{S37}$$

Integrating Kramers equation (S35) over time, we get

$$v\partial_x G - \partial_x U \partial_v G - \gamma \partial_v (vG + \partial_v G) = \delta(x)\mathcal{N}(v). \tag{S38}$$

Then, if we call $F\left(\widetilde{\widetilde{t}}\right)$ the exit time density, the mean exit time is simply

$$\widetilde{\widetilde{\tau}} = \int_0^{+\infty} d\widetilde{\widetilde{t}}\, \widetilde{\widetilde{t}}\, F\left(\widetilde{\widetilde{t}}\right). \tag{S39}$$

This first passage time density is related to the survival probability $S\left(\widetilde{\widetilde{t}}\right)$ through

$$F\left(\widetilde{\widetilde{t}}\right) = -\frac{dS}{d\widetilde{\widetilde{t}}}, \tag{S40}$$

and the survival probability can be deduced from the pdf

$$S\left(\widetilde{\widetilde{t}}\right) = \int_0^1 dx \int_{-\infty}^{+\infty} dv\, K\left(x, v, \widetilde{\widetilde{t}}\right). \tag{S41}$$

Using the definition of Green function and integrating by parts, we arrive at

$$\widetilde{\widetilde{\tau}} = \int_0^1 dx \int_{-\infty}^{+\infty} dv\, G(x, v). \tag{S42}$$

Following Ref. [7], we can decompose the velocity dependence of the Green function on the basis of rescaled harmonic oscillator eigenfunctions $\psi_n(v)$ as follows

$$G(x, v) = \psi_0(v) \sum_n c_n(x)\psi_n(v). \tag{S43}$$

The eigenfunctions $\psi_n(v)$ are related to the usual harmonic oscillator wavefunctions $\psi_n^H(v)$ by

$$\psi_n(v) = 2^{-1/4}\psi_n^H(2^{-1/2}v). \tag{S44}$$

For example, for $n = 0$, we have $\psi_0^H(v) = \pi^{-1/4} \exp\left(-\frac{v^2}{2}\right)$ and

$$\psi_0(v) = (2\pi)^{-1/4} \exp\left(-\frac{v^2}{4}\right). \tag{S45}$$

This function is related to the equilibrium velocity distribution $\mathcal{N}(v)$ through $\psi_0^2(v) = \mathcal{N}(v)$. The mean escape time can be written in terms of $c_0(x)$ as

$$\widetilde{\widetilde{\tau}} = \int dx\, dv\, G(x, v) = \int dx\, c_0(x) \tag{S46}$$

due to orthogonality relations between the ψ_n.

The advantage of this representation is that the coupling between neighboring modes $c_n(x)$ is proportional to γ^{-1} which allows, for periodic boundary conditions, to write an exact asymptotic expansion in the limit of strong damping γ. For our case, these equations read:

$$\begin{cases} \partial_x c_1 = \delta(x) \\ n\gamma c_n + \sqrt{n}(\partial_x + \partial_x U) c_{n-1} + \sqrt{n+1}\,\partial_x c_{n+1} = 0 \qquad \text{for } n \geq 1. \end{cases} \tag{S47}$$

In [7] these equations are then solved by continued fraction expansion which converges quickly even for small γ. Unfortunately this approach cannot be used here due to the boundary conditions. While the reflecting boundary conditions can still be written simply in the oscillator eigenfunction basis $c_n(0) = 0$ for odd n, the absorbing boundary conditions introduce a coupling between all the modes n. To see this, we rewrite the absorbing boundary condition $G(1, v) = 0$ for $v < 0$ in the ψ_n basis

$$c_{2n,0}(1) = \sum_m S_{nm} c_{2m+1,0}(1) \tag{S48}$$

where the coefficients S_{nm} are given by:

$$S_{nm} = 2 \int_0^\infty \psi_{2n}(v) \psi_{2m+1}(v) dv. \tag{S49}$$

The (infinite) matrix $\hat{S} = (S_{nm})$ is orthogonal $\hat{S}\hat{S}^t = \hat{I}$.

Using properties of Hermite functions [8], we found the asymptotic behavior of the first coefficients S_{0m}, S_{1m}

$$S_{0m} \sim \frac{(-1)^{m+1}}{\sqrt{2}\pi^{3/4} m^{5/4}} \tag{S50}$$

$$S_{1m} \sim \frac{(-1)^m \sqrt{3}}{2\pi^{3/4} m^{5/4}}. \tag{S51}$$

They decay quite slowly with m, thus in principle all the c_n modes are coupled and the property that c_n is of order γ^{-n} breaks down. However, we found that keeping only the first modes still provides an accurate numerical approximation (even if it is no longer an exact asymptotic development). Retaining the lowest modes, we truncate the hierarchy (S47) to

$$\begin{cases} \partial_x c_1 = \delta(x) \\ \gamma c_1 + \partial_x c_0 + \partial_x U c_0 + \sqrt{2}\partial_x c_2 = 0 \\ 2\gamma c_2 + \sqrt{2}\partial_x c_1 + \partial_x U \sqrt{2} c_1 = 0 \end{cases} \tag{S52}$$

and the boundary conditions to:

$$\begin{cases} c_1(0) = 0 \\ c_1(1) = S_{00} c_0(1) + S_{10} c_2(1) = \sqrt{\frac{2}{\pi}} c_0(1) + \frac{1}{\sqrt{\pi}} c_2(1). \end{cases} \tag{S53}$$

Solving this set of linear equations, and using $U(0) = U(1) = 0$, we obtain

$$c_0(x) = \gamma e^{-U(x)} \int_x^1 dy e^{U(y)} + \sqrt{\frac{\pi}{2}} \left(1 + \frac{U'(1)}{\sqrt{2\pi}\gamma}\right) e^{-U(x)} - \gamma^{-1} e^{-U(x)} \int_x^1 dy U''(y) e^{U(y)}. \tag{S54}$$

Coming back to the rescaling with t_d used in the main text and in the figures, we get

$$\widetilde{\tau} = \int_0^1 dx \int_x^1 dy e^{U(y)-U(x)} + \sqrt{\frac{\pi}{2}} \left(\frac{1}{\gamma} + \frac{U'(1)}{\sqrt{2\pi}\gamma^2}\right) \int_0^1 dx e^{-U(x)} - \frac{1}{\gamma^2} \int_0^1 dx \int_x^1 dy\, U''(y) e^{U(y)-U(x)}. \tag{S55}$$

VII. UNDERDAMPED TREATMENT: NUMERICS

The large-γ asymptotics derived above only provides a partial picture of the underdamped regime. To explore a larger range of frictions, we resort to numerics to evaluate the mean exit time associated to a general potential profile. In particular, we use finite element techniques to compute the Green function, defined in Eq. (S37), and that obeys

$$v\partial_x G - \partial_x U \partial_v G - \gamma \partial_v (vG + \partial_v G) = \delta(x)\mathcal{N}(v). \tag{S56}$$

To take the reflecting boundary conditions at $x = 0$ into account, we symmetrize the domain explored by the Brownian particles and add an absorbing wall at $x = -1$. The boundary conditions for G can then be written as $G(\delta\Omega) = 0$ where $\delta\Omega$ is the domain shown on Fig S6. The $G(x, v \to \pm\infty) = 0$ condition is replaced by a hard wall cut-off at $G(x, v = \pm V_\infty) = 0$. The peculiar shape of this domain is due to the fact that Kramers equation contains a derivative of order two in v but only first order derivatives in x [9].

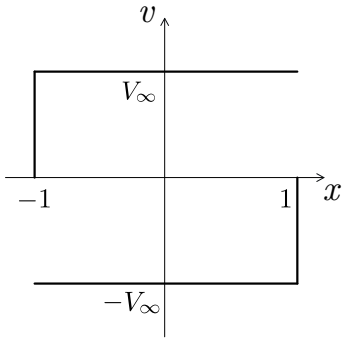

FIG. S6: Illustration of the domain $\delta\Omega$, constituted of the two portions of thick black line, on which the Green function is 0. The shape of the domain follows from Eq. (S56), which contains a second-order derivative in v but only first-order derivatives in x. Therefore two boundary conditions are needed in v, whereas only one is needed in x. In v, we simply use a cut-off $\pm V_\infty$. In x, the absorbing point at $x = 1$ prevents the particle to have a negative velocity at this point (as it would come from beyond this absorbing point), as well as the absorbing point at $x = -1$ prevents the particle from having positive velocity there.

To find G using a finite element method, we adopt the weak formulation given below where $\phi(x, v)$ is a trial function, and integration spreads over the entire domain in Fig. S6

$$\int \{\phi\,(v\partial_x G \,-\, \partial_x U\,\partial_v G) \,+\, \gamma v\, G\,\partial_v \phi \,+\, \gamma\,\partial_v \phi\,\partial_v G\}\,dv \,=\, \delta(x) \int \phi\,\mathcal{N} dv, \tag{S57}$$

as follows from Eq. (S56). We implemented this weak form using the FreeFem++ simulation package [10]. To test the numerical accuracy of the solutions obtained, we checked the conservation of current. For the exact solution, the current $J(x) = \int vG(x, v)dv$ is independent of x for all x on the same side of the source point. For our simulation parameters, the current was typically conserved with an accuracy $\sim 5\%$, with a maximal error of 15% for the lowest γ with which the convergence is the most difficult to achieve.

Once the mean exit time estimated through this finite element procedure for a given n-support potential profile, we use a simulated annealing algorithm, whose principle is the following. We pick at random one of the n vertices of the potential and change its U component by a random quantity in a predetermined range. This change is then accepted or rejected with a Metropolis procedure: if the new mean exit time, computed with finite elements, is smaller than the previous one, then the change is accepted. If it is higher, it is accepted with a probability

$$P_{\rm acc}\left(\tau_{\rm new}, \tau_{\rm old}, j\right) = \exp\left(-\frac{\tau_{\rm new} - \tau_{\rm old}}{T_j}\right) \tag{S58}$$

where T_j acts as a (computational) temperature, and is decreased as $1/j^2$ as the iteration step j increases. The algorithm is then stopped after a predetermined sufficiently high number of unsuccessful iterations (during which the mean exit time does not decrease).

[1] C. Gardiner, *Stochastic Methods: A Handbook for the Natural and Social Sciences* (2009).

[2] N. G. Van Kampen, *Stochastic processes in physics and chemistry*, vol. 1 (Elsevier, 1992).
[3] J.-L. Barrat and J.-P. Hansen, *Basic Concepts for Simple and Complex Liquids* (Cambridge University Press, 2003).
[4] V. V. Palyulin and R. Metzler, J. Stat. Mech. Theory Exp. **L03001** (2012).
[5] S. Pagliara, C. Schwall, and U. F. Keyser, Adv. Mater. **25**, 844 (2013).
[6] R. W. Bowman, G. M. Gibson, A. Linnenberger, D. B. Phillips, J. A. Grieve, D. M. Carberry, S. Serati, M. J. Miles, and M. J. Padgett, Comput. Phys. Commun. **185**, 268 (2014).
[7] H. Risken, in *The Fokker-Planck Equation* (Springer, 1996), pp. 63–95.
[8] S. Dvořák, Czechoslovak Journal of Physics B **23**, 1281 (1973).
[9] A. Araújo, A. K. Das, and E. Sousa, J. Phys. A: Math.and Theor. **48**, 045202 (2014).
[10] F. Hecht, J. Num. Math. **20** (2012).